Journal of Sound and Vibration 329 (2010) 1310–1331

Contents lists available at ScienceDirect

Journal of Sound and Vibration

journal homepage: www.elsevier.com/locate/jsvi

Detection of contiguous and distributed damage through contours of equal frequency change

N. Lakshmanan [a], B.K. Raghuprasad [b], N. Gopalakrishnan [a,*], K. Sathishkumar [a], S.G.N. Murthy [a]

[a] Structural Engineering Research Centre, CSIR Campus, Taramani, Chennai 600113, India
[b] Indian Institute of Science, Bangalore 560012, India

ARTICLE INFO

Article history:
Received 17 June 2009
Received in revised form
2 September 2009
Accepted 1 November 2009
Handling Editor: L.G. Tham
Available online 14 December 2009

ABSTRACT

The paper presents the results of a computational modeling for damage identification process for an axial rod representing an end-bearing pile foundation with known damage and a simply supported beam representing a bridge girder. The paper proposes a methodology for damage identification from measured natural frequencies of a contiguously damaged reinforced concrete axial rod and beam, idealized with distributed damage model. Identification of damage is from Equal_Eigen_value_change (Iso_Eigen_value_Change) contours, plotted between pairs of different frequencies. The performance of the method is checked for a wide variation of damage positions and extents. An experiment conducted on a free–free axially loaded reinforced concrete member and a flexural beam is shown as examples to prove the pros and cons of this method.

1. Introduction

Countries world-over have thousands of critical structures and bridges which have been built decades back when strength-based designs were the order of the day. Over the years, magnitude and frequency of loadings on these have increased. Also, these structures have been exposed to environmental degradation during their service life. Hence, structural health monitoring (SHM) has attracted the attention of researchers, world over. Structural health monitoring is recommended both for vulnerable old structures as well as for new important structures. The methodology adopted for damage identification should be simple, both in terms of investigations involved and the instrumentation. Health monitoring with global damage indicators and inference of the health of the structure should involve easier and simple instrumentation capable of remotely capturing the data. The paper presents a natural frequency change based damage identification strategy with modification in the acclaimed Cawley–Adams criterion such that this may be adopted for pile foundations and simply supported bridges.

The pioneering work and the resulting classical Cawley–Adams criterion states that the ratio of frequency change in two modes is only a function of the damage location and independent of the damage magnitude [1]. The other connected papers, which inspire the present work, include that of Morassi [2], Palacz and Krawczuk, [3,4], Krawczuk et al. [5], Krawczuk et al. [6], Krawczuk [7] and Gladwell's [8] classical book. The present paper develops relevant expressions and design-aid like contours for damage identification for distributed damage scenario as encountered in the case of reinforced

* Corresponding author. Tel.: +91 44 22549145; fax: +91 44 22541508.
E-mail address: ng@sercm.org (N. Gopalakrishnan).

0022-460X/$ - see front matter © 2009 Elsevier Ltd. All rights reserved.
doi:10.1016/j.jsv.2009.11.006

concrete or pre-stressed concrete structures. Relevant equations for smeared damage model and the resulting solutions are also discussed. Typical experiments conducted on reinforced concrete simply supported beams and their comparison show the robustness of the developed method and relevant recommendations are made.

The other papers in this field are described subsequently and by no-means the list is exhaustive. A comprehensive survey on damage detection through vibration testing is presented by Doebling et al. [9]. Experiments and analytical predictions conducted by Owolobi et al. [10] and Yang et al. [11] provide benchmark data for researchers in this field. Silva and Gomes [12] have used slotted and fatigue-cracked beams in experimental modal analyses. Cracks in a cantilever beam are modeled as a fracture hinge by Ju and Mimovich [13]. Reinforced and plain concrete beams are tested by Choudhury and Ramirez [14] where changes in resonant frequencies and power spectral densities of displacements resulting from simulated damage are studied. Polycarbonate cantilever beam having an opening and closing crack in the interior of the beam, running parallel to the top and bottom surfaces is studied by Prime and Shevitz [15]. Lakshmanan et al. [16] and Rajagopalan et al. [17] have correlated the cracking and yielding stiffness of the normal and fiber-reinforced concrete beams, under various stages of pre-loading with the fundamental frequencies. A method is outlined such that from frequency measurements, maximum load carried by the bridge in its life time could be estimated. Hassiotis and Jeong [18] and Hassiotis [19] outlined a method based on first order perturbation and optimization theory to compute the damage from measured natural frequencies.

Recently, wavelet based damage detection technique, which makes use of dynamic and static response and using ANN techniques are dealt with by Lakshmanan et al. [20–23].

In a recent paper by Yu et al. [24], the Eigen value perturbation theory is introduced to obtain the Eigen values and Eigen vectors of the damaged structure for reducing the computation load. Two artificial neural networks (ANN) schemes are trained based on the response data simulated using finite element method (FEM) and perturbation theory enhanced finite element method (PFEM), respectively.

2. Natural frequency change as a perturbation problem—axial rod [25]

A perturbation analysis of the non-degenerate dynamic system with small perturbations occurring in its stiffness and mass matrices is made use of to derive the appropriate equations.

The unperturbed (zeroth-order) problem is:

$$K_0 p_i^{(0)} = \lambda_i^{(0)} M_0 p_i^{(0)} \tag{1}$$

$\mathbf{K_0}$ and $\mathbf{M_0}$ are the stiffness and mass matrices at the initial state and $\lambda_i^{(0)}$ and $\mathbf{p_i^{(0)}}$ are the corresponding i-th Eigen value and vector. If $\mathbf{K_1}$ and $\mathbf{M_1}$ be the small perturbations in stiffness and mass matrices, respectively, then the perturbed problem could be written as

$$(K_0 + K_1) p_i = \lambda_i (M_0 + M_1) p_i \tag{2}$$

The Eigen values and vectors can be expanded in terms of a parameter γ, such that zeroth, first, etc., powers of γ correspond to the zeroth, first orders of perturbation analysis. The perturbed portion of the original matrix, namely $\mathbf{K_1}$ and $\mathbf{M_1}$ can be replaced by $\gamma \cdot \mathbf{K_1}$ and $\gamma \cdot \mathbf{M}_1$ and λ_i and $\mathbf{p_i}$ are expressed as power series in γ.

The perturbed Eigen values and vectors are written as

$$\lambda_i = \lambda_i^{(0)} + \gamma \cdot \lambda_i^{(1)} + \gamma^2 \cdot \lambda_i^{(2)} + \cdots$$

$$p_i = p_i^{(0)} + \gamma \cdot p_i^{(1)} + \gamma^2 \cdot p_i^{(2)} + \cdots \tag{3}$$

By substituting the perturbed Eigen values and vectors into Eq. (2), one obtains the following modified Eigen value problem:

$$(K_0 + \gamma \cdot K_1)(p_i^{(0)} + \gamma \cdot p_i^{(1)} + \gamma^2 \cdot p_i^{(2)} + \cdots) = (\lambda_i^{(0)} + \gamma \cdot \lambda_i^{(1)} + \gamma^2 \cdot \lambda_i^{(2)} + \cdots)(M_0 + \gamma \cdot M_1)(p_i^{(0)} + \gamma \cdot p_i^{(1)} + \gamma^2 \cdot p_i^{(2)} + \cdots) \tag{4}$$

After equating coefficients of equal powers of γ on both sides of the equation, we can write the zeroth, first and higher order perturbation equations. These are

$$K_0 p_i^{(0)} = \lambda_i^{(0)} M_0 p_i^{(0)}$$

$$K_0 p_i^{(1)} + K_1 p_i^{(0)} = \lambda_i^{(0)} M_0 p_i^{(0)} + \lambda_i^{(0)} M_1 p_i^{(0)} + \lambda_i^{(1)} M_0 p_i^{(0)} \tag{5}$$

It is seen that zeroth order problem is the unperturbed problem. The vector $\mathbf{p_i^{(1)}}$ can be expanded on the basis of unperturbed Eigen vectors and may be written as

$$p_i^{(1)} = \sum_r c_{ir} p_r^{(0)} \tag{6}$$

The scalar c_{ir} is the scaling factor, with which the original mode shapes are modified to render perturbed mode shapes. After simplification and imposing ortho-normalizing properties for both old and new Eigen vectors, the first order

perturbation calculations of i-th Eigen values and vectors can be written as

$$\lambda_i = \lambda_i^{(0)} + p_i^{(0)\mathrm{T}}(K_1 - \lambda_i^{(0)} M_1) p_i^{(0)}$$

$$p_i = p_i^{(0)} - \left(\frac{1}{2} p_i^{(0)\mathrm{T}} M_1 p_i^{(0)}\right) \cdot p_i^{(0)} + \sum_{\substack{r=1 \\ r \neq i}}^{n} \left(\frac{p_r^{(0)\mathrm{T}}(K_1 - \lambda_i^{(0)} M_1) p_i^{(0)}}{\lambda_i^{(0)} - \lambda_r^{(0)}}\right) \cdot p_r^{(0)} \tag{7}$$

For the condition of a damaged structure, wherein the mass matrix does not undergo any change from the original matrix, the above equation can be further simplified as

$$\lambda_i = \lambda_i^{(0)} + p_i^{(0)\mathrm{T}} K_1 p_i^{(0)}$$

$$p_i = p_i^{(0)} + \sum_{\substack{r=1 \\ r \neq i}}^{n} \left(\frac{p_r^{(0)\mathrm{T}} K_1 p_i^{(0)}}{\lambda_i^{(0)} - \lambda_r^{(0)}}\right) \cdot p_r^{(0)} \tag{8}$$

$\lambda_i, \lambda_i^{(0)}$ is the Post and Pre damage i-th Eigen values, $\mathbf{p}_i, \mathbf{p}_i^{(0)}$ the Post and Pre damage i-th Eigen vectors, $\mathbf{K}_1$ the Perturbation content of the stiffness matrix (Sparse).

From the above expressions, it can be noted that only the i-th un-perturbed parameters enter into the calculations of perturbed Eigen values, whereas the complete un-perturbed Eigen solution is required for the computation of perturbed Eigen vectors. The insights from the above equation is that: "The change in Eigen value due to a damage is equivalent to twice the strain energy release in the damaged zone, under the action of an ortho-normalised displacement profile".

3. Eigen value changes due to damage for an axial rod element

The strain energy equation for axial rod (Fig. 1) element is given by

$$U = \frac{1}{2} \int_0^{\ell} AE \left(\frac{\partial u}{\partial x}\right)^2 \cdot \mathrm{d}x \tag{9}$$

where, the mode shape is $u_{(x)} = \sin(2k-1)(\pi x/2\ell)$ which corresponds to the initial un-damaged state. The natural frequency for undamaged axial structural element is given by

$$f_{ud} = (2k-1)\frac{\pi}{2}\sqrt{\frac{EA}{M\ell}} \tag{10}$$

The reduction in Eigen values can be obtained as

$$\Delta f_d^2 = \frac{\beta AE(2k-1)^2\pi^2}{4\ell(0.5M)} \left[\frac{b_0}{\ell} + \frac{1}{(2k-1)\pi}\left\{\sin\frac{(2k-1)\pi b_0}{\ell} \cdot \cos\frac{(2k-1)\pi \ell_0}{\ell}\right\}\right] \tag{11}$$

where, αAE in Fig. 1 is the existing axial rigidity AE after the damage, resulting in a loss of βAE. Such that $1-\alpha=\beta$.

For a widespread uniform reduction in AE, substituting, $l_0=b_0=l/2$:

$$\Delta f_d^2 = \frac{\beta AE(2k-1)^2\pi^2}{4\ell M} \tag{12}$$

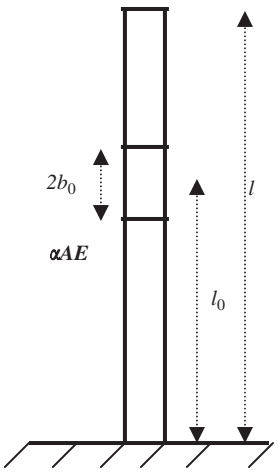

Fig. 1. An axial rod element supported at one end, with a discrete defect.

The ratio of Eigen value reduction is

$$\frac{\Delta f_d^2}{f_{ud}^2} = 2\beta\left[\frac{b_0}{\ell} + \frac{1}{(2k-1)\pi}\left\{\sin\frac{(2k-1)\pi b_0}{\ell}\cdot\cos\frac{(2k-1)\pi\ell_0}{\ell}\right\}\right] \tag{13}$$

4. Damage identification from Equal_Eigen_Value_Change contours and case studies

Ratio of the changes in Eigen values (between 'k-th' and 'n-th' modes) are obtained after modifying and re-writing Eq. (13) as

$$\frac{\Delta f_{d,k}^2 \cdot f_{ud,n}^2}{f_{ud,k}^2 \cdot \Delta f_{d,n}^2} = \frac{\left[\frac{b_0}{\ell} + \frac{1}{(2k-1)\pi}\left\{\sin\frac{(2k-1)\pi b_0}{\ell}\cdot\cos\frac{(2k-1)\pi\ell_0}{\ell}\right\}\right]}{\left[\frac{b_0}{\ell} + \frac{1}{(2n-1)\pi}\left\{\sin\frac{(2n-1)\pi b_0}{\ell}\cdot\cos\frac{(2n-1)\pi\ell_0}{\ell}\right\}\right]} \tag{14}$$

It is thus proved that the ratio of changes in Eigen values (squared frequencies) are independent of the magnitude of damage and are functions of only the central position of damage and its extent. Indirectly, the method is to find out the ratio of variation in frequencies as the normalizing factor, f_k^2/f_n^2, is only $(2k-1)^2/(2n-1)^2$, which is a constant for any pair of frequencies. Having eliminated a variable (β), out of three, it is possible to construct curves such that the variation of Eigen-value_change-ratios can be visualized. Varying values of $2b_0/\ell, \ell_0/\ell$ which give rise to constant Eigen-value-change-ratios $(\Delta\omega_n^2/\Delta\omega_m^2)(\omega_m^2/\omega_n^2)$, for an end-bearing axial rod are plotted in the form of contours. Figs. 2–4 show the contours of equal Eigen-value-change-ratios, for pairs of Eigen values namely 2-1 (k=2, n=1), 3-1 and 4-1, respectively. The curves are generated for a rod of 200 segments.

The exercise is not just a theoretical one and certain physical in-sights are obtained:

(a) Contours are un-symmetrical about the centre.
(b) The boundary line shows that the extent of damage $2b_0/\ell$, on the Y-axis shall at best be twice the centre of damage location ℓ_0/ℓ, on the X-axis.
(c) Contours at the centre of the figure, indicate a constant damage and all frequencies are affected equally and hence the ratio is 1.0.
(d) Contours closer to free end are around 3–4, indicating that high frequencies are affected more by off-centric damage near the free-end.

This exercise on the theoretical damage identification study involves certain example problems which are solved using these contours.

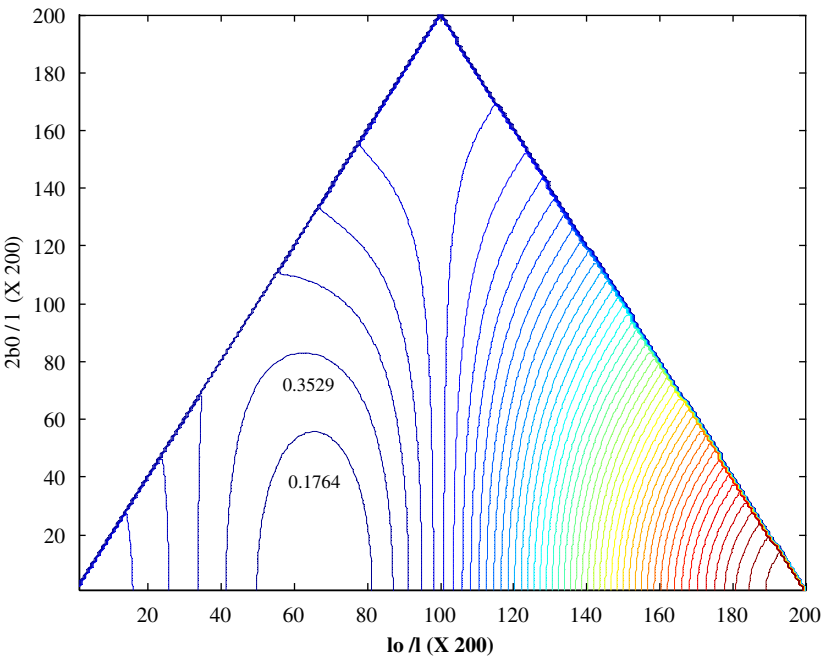

Fig. 2. Iso-Eigen-value_Change contours for frequency ratio 2:1 (Increment: 0.17643).

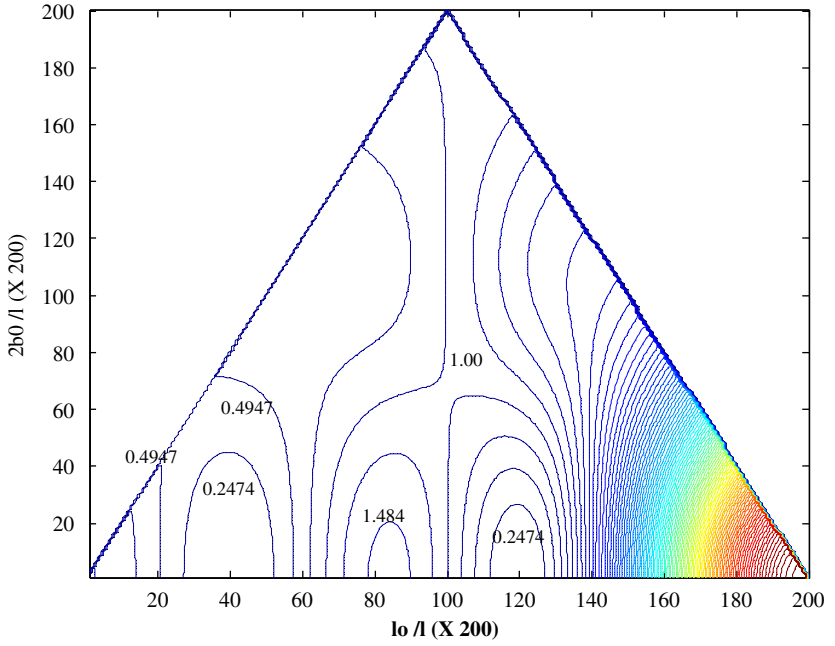

Fig. 3. Iso-Eigen-value_Change contours for frequency ratio 3:1 (Increment: 0.247354).

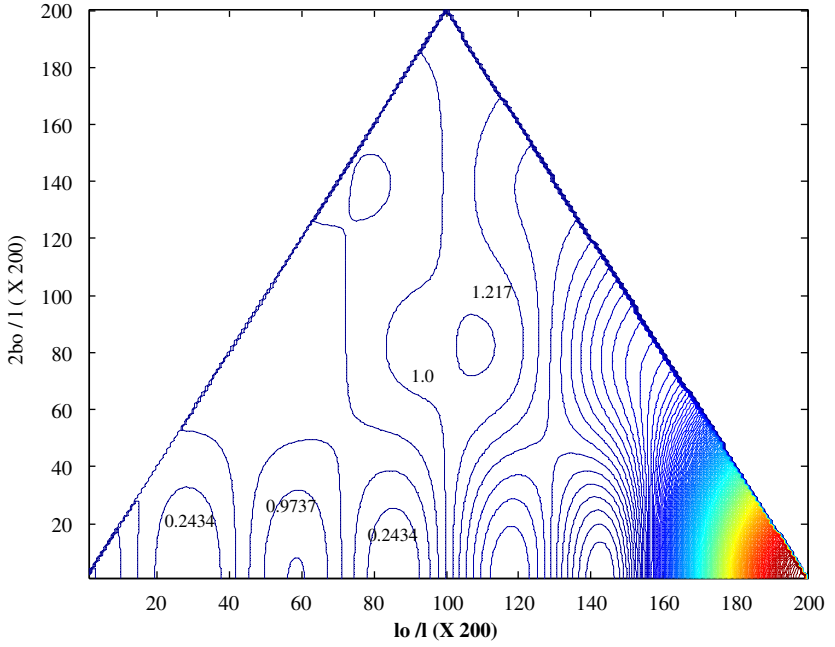

Fig. 4. Iso-Eigen-value-Change contours for frequency ratio 4:1 (Increment: 0.243445).

The six example validation problems solved are as follows (β is the magnitude of damage, kept as 0.10):

(a) $\frac{2b_0}{\ell}=0.1,\frac{\ell_0}{\ell}=0.25,\beta=0.1$ (b) $\frac{2b_0}{\ell}=0.2,\frac{\ell_0}{\ell}=0.25,\beta=0.1$ (Fig. 5)

(c) $\frac{2b_0}{\ell}=0.10,\frac{\ell_0}{\ell}=0.75,\beta=0.1$ (d) $\frac{2b_0}{\ell}=0.20,\frac{\ell_0}{\ell}=0.75,\beta=0.1$ (Fig. 6)

(e) $\frac{2b_0}{\ell}=0.10,\frac{\ell_0}{\ell}=0.4,\beta=0.1$ (f) $\frac{2b_0}{\ell}=0.20,\frac{\ell_0}{\ell}=0.4,\beta=0.1$ (Fig. 7)

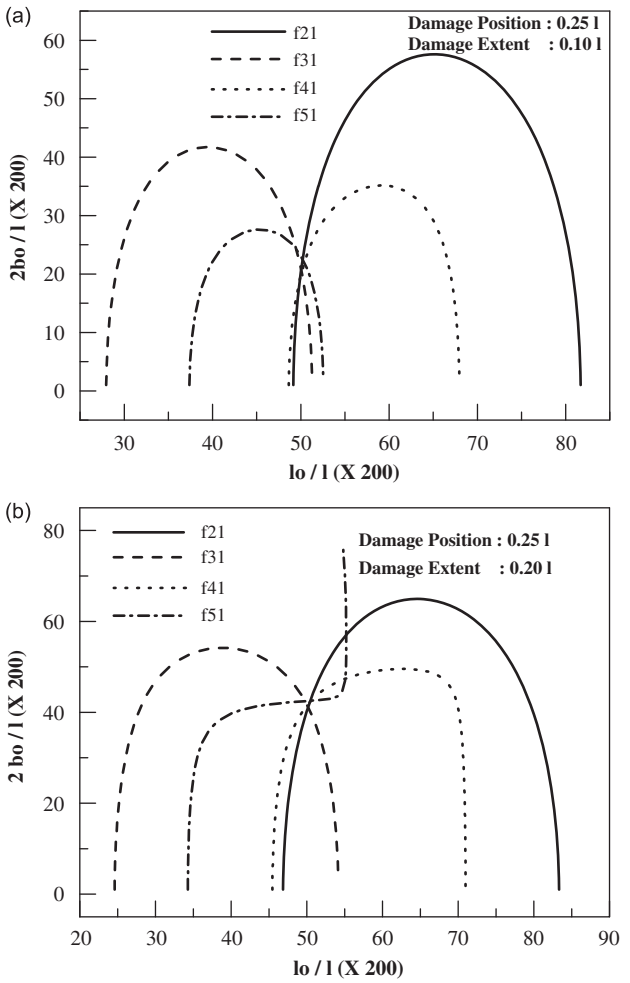

Fig. 5. Damage identification using Iso_Eigen value change contours: damage position: 0.25 l: (a) extent 0.10 l; (b) 0.20 l.

The intersection point of all the contours indicate the position and extent of damage, and Figs. 5–7 give the results of all the cases. After the geometric details of the damage are got, Eq. (12) is used to extract the magnitude of damage. The least square estimation can be adopted, for this over-determined set of equations, (with more equations and less un-known).

The first note of caution is that the formulation generally deals with un-damped frequencies. However, since only the ratio of frequencies is required, if damping remains the same for all modes before and after damage, the formulation still hold good. In a case where different modes are associated with different damping ratios, then suitable modifications are required in the expressions developed.

Another note of caution is due to the magnitude of damage. It is found that Eigen value change is a linear function of damage magnitude β, only up to 30% of damage. Hence identification of damage magnitude will be erroneous for large magnitudes of damage. However, it may be surmised that, since extent and position of damage involves Eigen-value change ratios, these two factors might be tolerant to a slightly higher values of β.

5. Natural frequency change as a perturbation problem—simply supported beam

From Eq. (8), it can be noted that only the i-th un-perturbed Eigen parameters enter into the calculations of perturbed Eigen values, whereas the complete unperturbed Eigen solution is required for the computation of the perturbed Eigenvectors. The perturbation equation states that the new values of frequencies can be obtained by using the original unperturbed Eigen functions:

$$\omega_d^2 = \frac{\displaystyle\int_0^{\ell_0-b_0} EI\cdot\left(\frac{\mathrm{d}^2y}{\mathrm{d}x^2}\right)^2\mathrm{d}x+\int_{\ell_0-b_0}^{\ell_0+b_0}\alpha EI\cdot\left(\frac{\mathrm{d}^2y}{\mathrm{d}x^2}\right)^2\mathrm{d}x+\int_{\ell_0+b_0}^{\ell} EI\cdot\left(\frac{\mathrm{d}^2y}{\mathrm{d}x^2}\right)^2\mathrm{d}x}{\displaystyle\int_0^{l}\overline{m}y^2\,\mathrm{d}x} \tag{15}$$

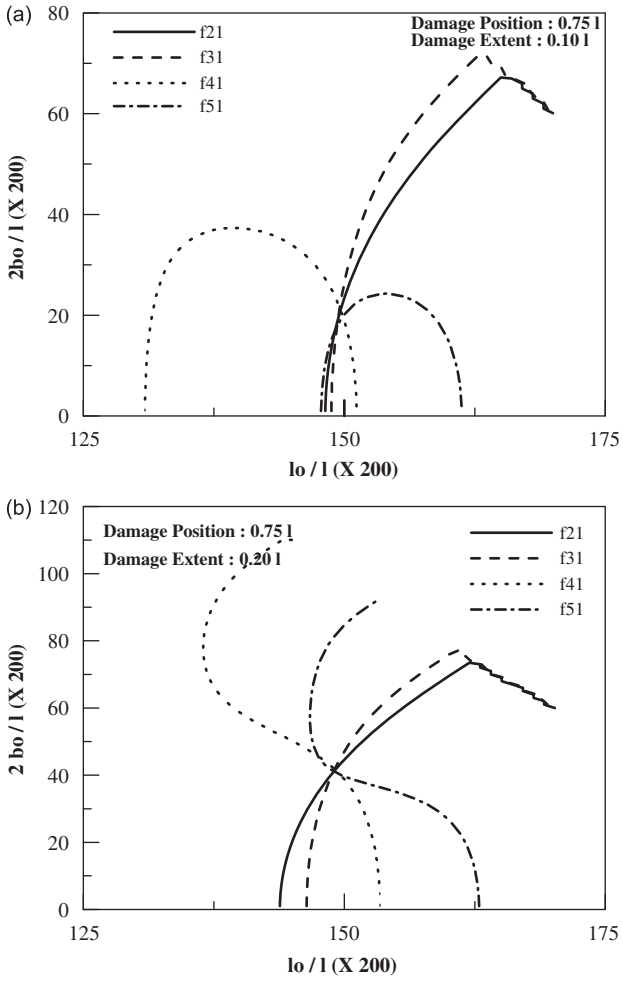

Fig. 6. Damage identification using Iso_Eigen value change contours: damage position: 0.75 l: (a) extent 0.10 l; (b) 0.20 l.

where $y_n(x)=\sin(n\pi x/\ell)$ is the mode shape corresponding to the initial state. By making a substitution of $\beta=1-\alpha$, $0\leq\alpha\leq1$, (where α is the ratio of the damaged *EI* as compared to the original *EI* and β is the magnitude of damage) in the previous equation and simplifying, the following expression for the normalized natural frequency is obtained for the damaged simply supported beam:

$$\left(\frac{\omega_d}{\omega}\right)_n=\sqrt{1-2\beta\left[\frac{b_0}{\ell}-\frac{1}{2n\pi}\left(\cos\frac{2n\pi\ell_0}{\ell}\cdot\sin\frac{2n\pi b_0}{\ell}\right)\right]} \tag{16a}$$

$$\left(\frac{\Delta\omega^2}{\omega^2}\right)_n=2\beta\left[\frac{b_0}{\ell}-\frac{1}{2n\pi}\left(\cos\frac{2n\pi\ell_0}{\ell}\cdot\sin\frac{2n\pi b_0}{\ell}\right)\right] \tag{16b}$$

For the case of a beam (Fig. 8) with a uniform reduction of *EI* to αEI for its entire length, the equation reduces to a simplest case possible:

$$\left(\frac{\omega_d}{\omega}\right)_n=\sqrt{1-\beta}=\sqrt{\alpha} \tag{17}$$

If further simplifications are made in the foregoing equation for the case of a crack situated at the centre and for values of b_0 tending towards zero:

$$\left(1-\left(\frac{\omega_d}{\omega}\right)^2\right)_n\cong\frac{2\beta\cdot b_0}{\ell}[1-(-1)^n] \tag{18}$$

Eq. (18) states that for a centrally situated defect, with length closer to zero, even-numbered modes have no reduction in their frequencies. The above set of equations, though approximate and simple and based on a first order perturbation

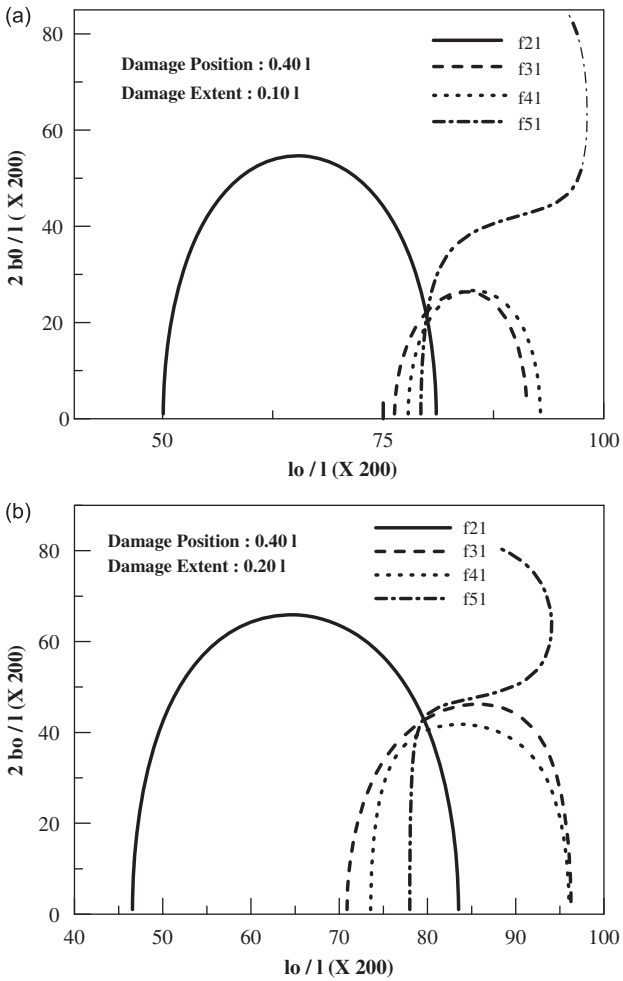

Fig. 7. Damage identification using Iso_Eigen value change contours: damage position: 0.40 l; (a) extent 0.10 l and (b) 0.20 l.

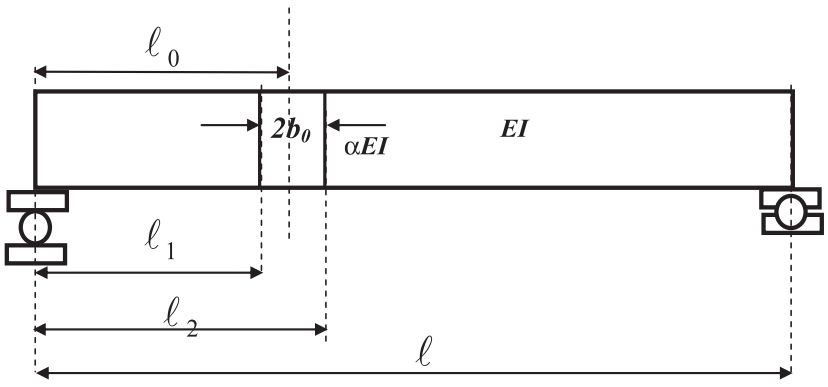

Fig. 8. Simply supported beam with a reduced *EI* for portion of its length.

theory, sheds insights into some concepts as summarized below:

(a) The defect in a beam manifested in the form of a reduction in its fundamental frequencies is a function of (i) position of damage l_0, (ii) extent of damage $2b_0$ and (iii) the magnitude of damage β.
(b) The position of damage is such that it is sensitive to certain set of frequencies only. The simple example is the invariance of even numbered modes to a centrally situated damage.

(c) The upper-bound of the reduced frequency for a magnitude of damage β is at best $\sqrt{\beta}$, when the reduction in *EI* is full and widespread. In all other cases it is less than this value. However for a total uniform reduction in *EI*, the mode shape does not change from the original state.

6. Damage identification from equal Eigen_Value_Change contours and case studies

Ratio of the changes in Eigen values are obtained after modifying and re-writing Eq. (16b) as

$$\frac{\Delta\omega_n^2}{\Delta\omega_m^2}\frac{\omega_m^2}{\omega_n^2}=\frac{\Delta\omega_n^2}{\Delta\omega_m^2}\frac{m^4}{n^4}=\frac{\left[\frac{b_0}{\ell}-\frac{1}{2n\pi}\left(\cos\frac{2n\pi\ell_0}{\ell}\cdot\sin\frac{2n\pi b_0}{\ell}\right)\right]}{\left[\frac{b_0}{\ell}-\frac{1}{2m\pi}\left(\cos\frac{2m\pi\ell_0}{\ell}\cdot\sin\frac{2m\pi b_0}{\ell}\right)\right]} \tag{19}$$

It is thus proved that the ratio of changes in Eigen values (squared frequencies) are independent of the magnitude of damage and are functions of only the central position of damage and its extent. Indirectly, the method is to find out the ratio of variation in frequencies as the normalizing factor, ω_m^2/ω_n^2, is only m^4/n^4, which is a constant for any pair of frequencies. Having eliminated a variable (β), out of three, it is possible to construct curves such that the variation of Eigen-value_change-ratios can be visualized. Varying values of $2b_0/\ell, \ell_0/\ell$ which give rise to constant Eigen-value_change-ratios $(\Delta\omega_n^2/\Delta\omega_m^2)(\omega_m^2/\omega_n^2)$, for a simply supported beam are plotted in the form of contours. Figs. 9–11 show the contours of equal Eigen-value-change-ratios, for pairs of Eigen values namely 2-1 (n=2, m=1), 4-2 and 3-1, respectively. The curves are generated for a beam of 500 segments.

The exercise is not just a theoretical one and certain physical in-sights are obtained:

(a) Contours are symmetrical indicating that a symmetrical damage affects the frequencies equally.
(b) The boundary line shows that the extent of damage $2b_0/\ell$, on the *Y*-axis shall at best be twice the centre of damage location ℓ_0/ℓ, on the *X*-axis.
(c) Contours at the top most point of the figure, indicate a wide-spread constant damage and all frequencies are affected equally and hence the ratio is 1.0.
(d) Contours closer to support are around 3–4, indicating that high frequencies are affected more by off-centric damage.
(e) As a converse of point (d), contours closer to mid-span, for 21, 31 and 41 contours show smaller values especially for small amounts of damage.

This exercise on the theoretical damage identification study involves certain example problems which are solved using these contours.

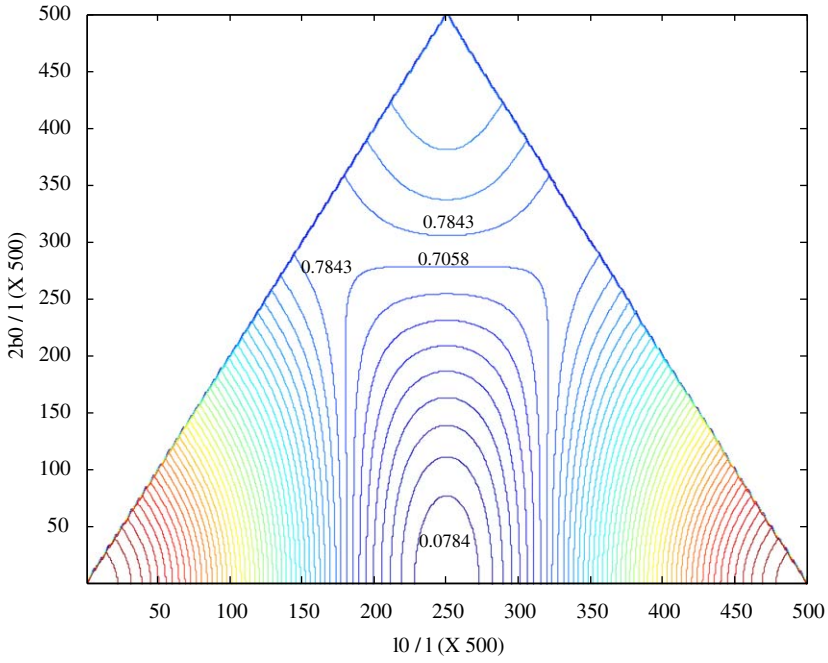

Fig. 9. Iso-Eigen-value-Change contours for frequency ratio 2:1 (Increment: 0.07843).

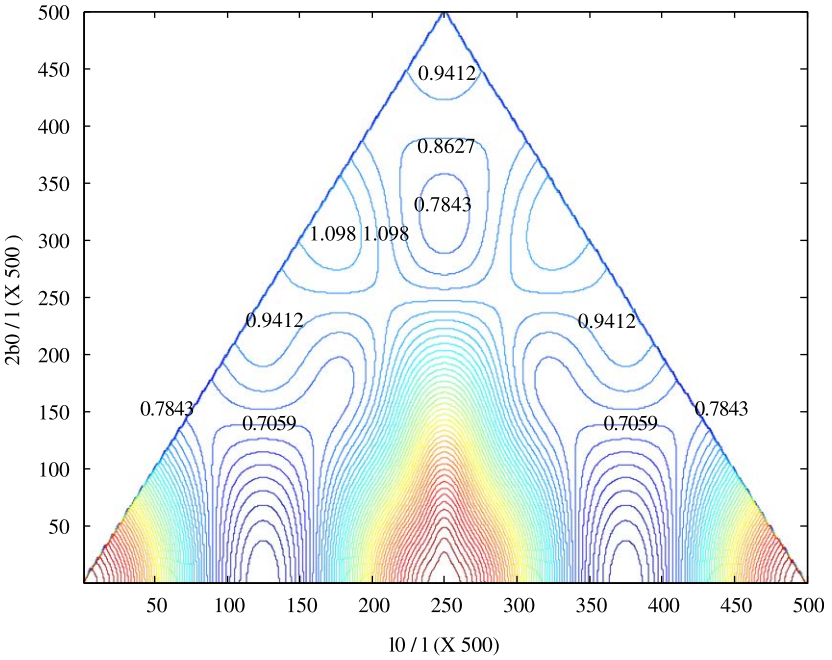

Fig. 10. Iso-Eigen-value Change contours for frequency ratio 4:2 (Increment: 0.07843).

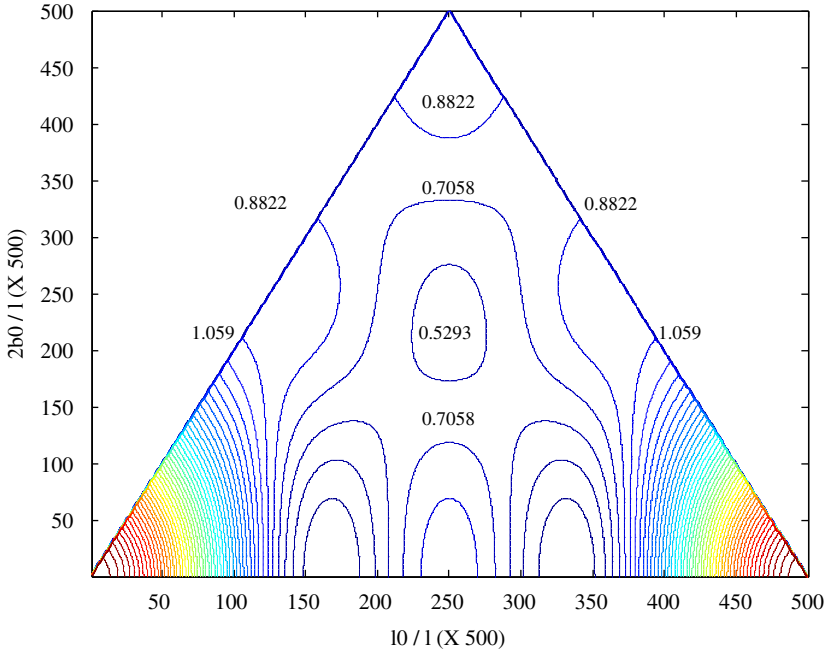

Fig. 11. Iso-Eigen-value-Change contours for frequency ratio 3:1 (Increment: 0.1764).

The six example validation problems solved are as follows (β is the magnitude of damage, kept as 0.10):

$$\text{(a) } \frac{2b_0}{\ell}=0.1,\frac{\ell_0}{\ell}=0.25,\beta=0.1 \quad \text{(b) } \frac{2b_0}{\ell}=0.3,\frac{\ell_0}{\ell}=0.25,\beta=0.1$$

$$\text{(c) } \frac{2b_0}{\ell}=0.10,\frac{\ell_0}{\ell}=0.144,\beta=0.1 \quad \text{(d) } \frac{2b_0}{\ell}=0.20,\frac{\ell_0}{\ell}=0.144,\beta=0.1$$

$$\text{(e) } \frac{2b_0}{\ell}=0.30,\frac{\ell_0}{\ell}=0.5,\beta=0.1 \quad \text{(f) } \frac{2b_0}{\ell}=0.20,\frac{\ell_0}{\ell}=0.5,\beta=0.1$$

It is seen than case (a) to case (d) are un-symmetrical damage patterns and case (e) and case (f) are symmetrical damages. For example, in case (a) $(\Delta\omega_n^2/\Delta\omega_m^2)(\omega_m^2/\omega_n^2)$ for the pairs of 2-1, 4-2, 3-1 and 4-1 frequency ratios are 1.897, 0.129, 0.968 and 0.245, respectively. The intersection point of all the contours indicate the position and extent of damage, which in this case works out to be 0.25 and 0.1, respectively (Fig. 12(a)). Figs. 12(b)–(f) show the results of the remaining cases namely (b)–(f). After the geometric details of the damage are got, Eq. (16b) is used to extract the magnitude of

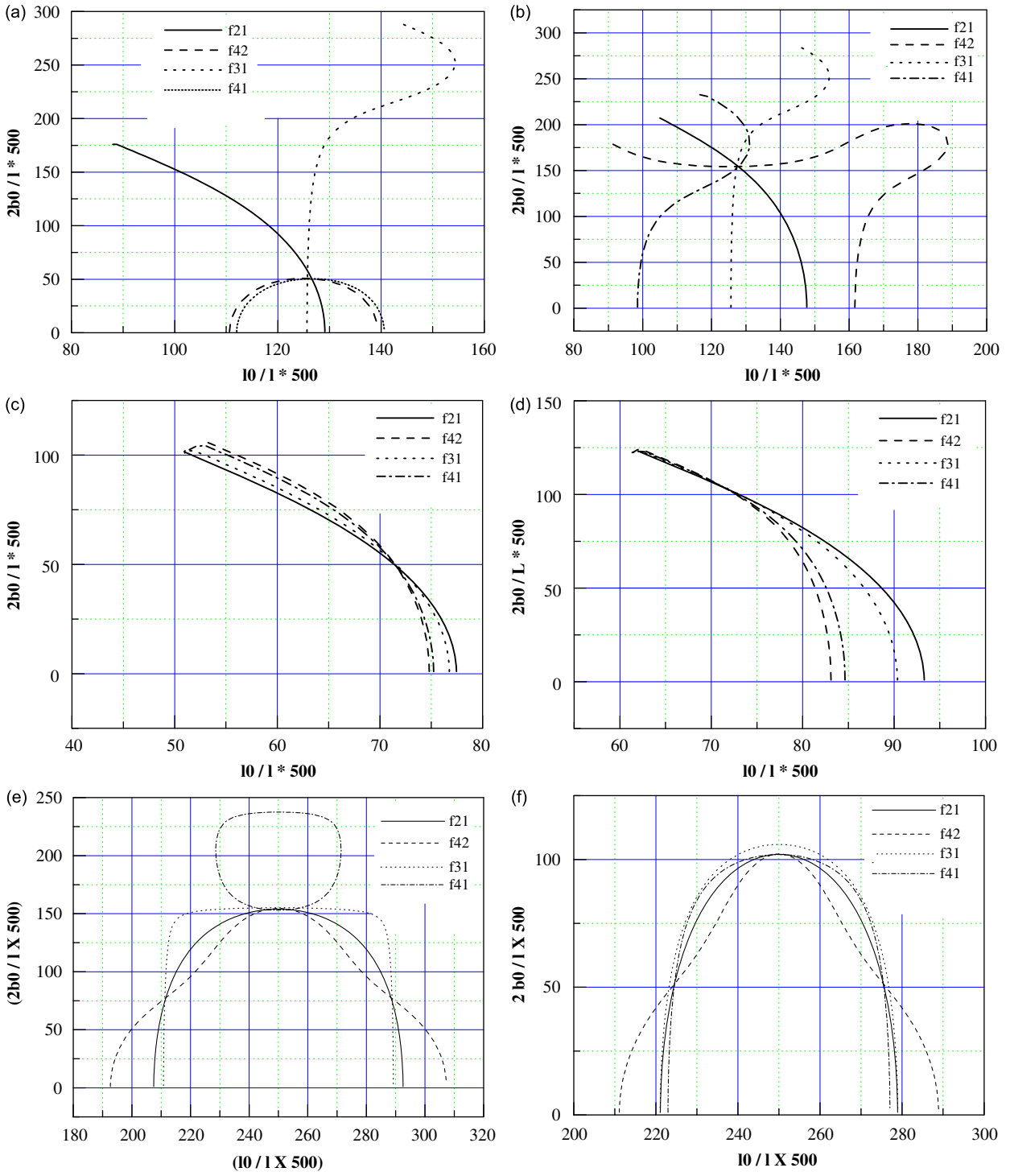

Fig. 12. Prediction of damage position and extent from Iso_Eigen_value change contours, for damage patterns D1–D6: (a) D1; (b) D2; (c) D3; (d) D4; (e) D5; (f) D6.

damage. The least square estimation can be adopted, for this over-determined set of equations, (with four equations and one un-known), which in this case works out to be 0.10.

It is to be observed that, for symmetrical damages, the intersection point is also a point of zero slope and hence the contours are tangential to each other. In Fig. 12(e), a symmetrical case requires contour information from 4-1 frequency pair to resolve the exact intersection point, otherwise ℓ_0/ℓ is predicted as 0.42 as against 0.50. However, Fig. 12(f) shows two intersection points ℓ_0/ℓ equal to 0.45 in addition to 0.5. An extra frequency information may be required to resolve this issue or additionally, the authors propose a static based system identification procedure [23], which shall resolve a symmetric and an un-symmetric damage, in conjunction with dynamic measurements.

7. Effect of error bounds on Iso-Eigen_value_Change contours

An extension of this work is the study of the performance of this damage identification methodology, with errors in frequency ratios. The previously mentioned case studies, namely

$$\text{(a) } \frac{2b_0}{\ell}=0.1,\frac{\ell_0}{\ell}=0.25,\beta=0.1 \quad \text{(b) } \frac{2b_0}{\ell}=0.3,\frac{\ell_0}{\ell}=0.25,\beta=0.1$$

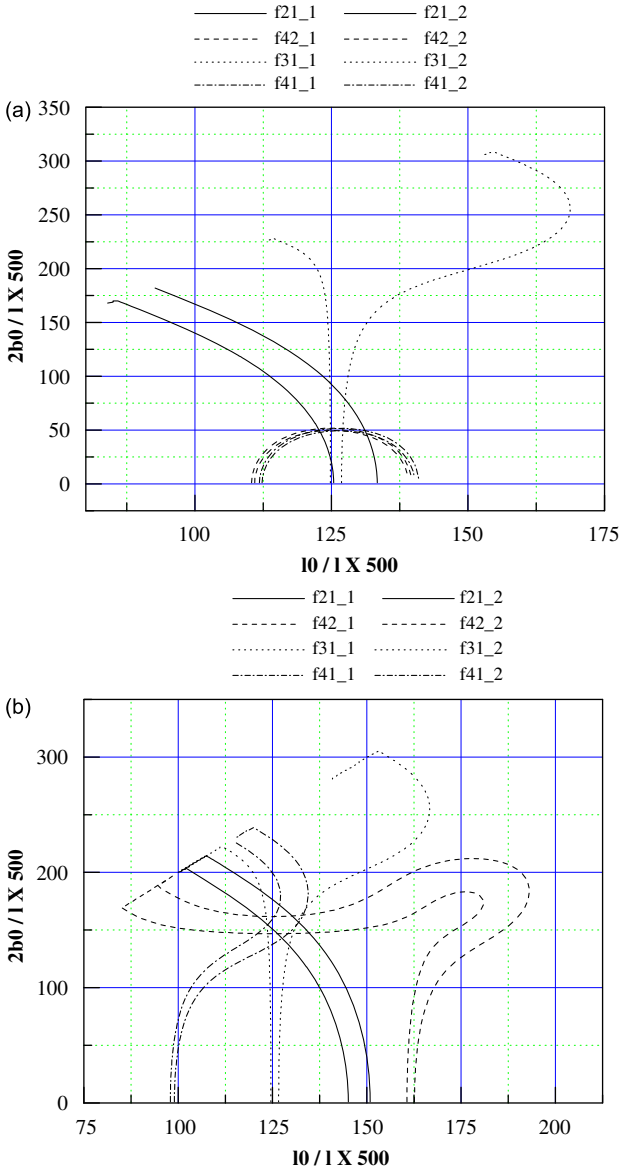

Fig. 13. Prediction of damage position and extent with 5% error bounds from Iso_Eigen_value-change contours: (a) D1; (b) D2.

are repeated with error bounds in measurements. For example, an error bound of $\pm 5\%$ is introduced artificially on each of these contour plots. This means that the previously generated contours, would have given rise to a fresh pair of contours of values 0.95 and 1.05 times the original values. All the eight curves are super-imposed and shown for these two cases (Figs. 13a and b). The inference is that, even though the region of intersection has widened, divergence of results is not seen and the centre of the intersected area is still the actual damaged point. Also it is to be noted that errors of 5% magnitudes are rather large. Ideally typical source or error is the change in the frequency, for a small extent of damage situated in a node position of a beam, thus giving a small change in $\Delta\omega^2$. This coupled with the frequency resolution in FFT, may end up giving a larger error.

8. Evaluation of extent of damage for a symmetric damage

We shall try to resolve the problems in identification of symmetrical central damage from the iso_Eigen-value_change contours by resorting to another related method. Supposing that an a-priori knowledge exists such that the likely damage onto a structure is symmetric, distributed and centrally located, the fact is advantageously utilized to estimate both the extent of damage and the magnitude. We shall revert back to Eq. (16b) and simplify the same for symmetric damages:

$$\left(\frac{\Delta\omega^2}{\omega^2}\right)_n = \frac{2\beta \cdot b_0}{\ell}\left[1 - \frac{\ell}{2n\pi b_0}(-1)^n \sin\frac{2n\pi b_0}{\ell}\right] \tag{20a}$$

$$\left(\frac{\Delta\omega^2}{\omega^2}\right)_n = \frac{2\beta \cdot b_0}{\ell}[1 - (-1)^n \sin c(n\pi x)]; x = \frac{2b_0}{\ell} \tag{20b}$$

$$\frac{\Delta\omega_n^2\omega_m^2}{\omega_n^2\Delta\omega_m^2} = \frac{1 - (-1)^n \sin c(n\pi x)}{1 - (-1)^m \sin c(m\pi x)} \tag{20c}$$

Between the third and first modes, the equation is further simplified as

$$\frac{\Delta\omega_3^2}{81\Delta\omega_1^2} = \frac{1 + \sin c(3\pi x)}{1 + \sin c(\pi x)} \tag{20d}$$

Eq. (20d) is plotted in Fig. 14 and the horizontal intersection point on this bell-shaped curve for an Eigen_value_change_ratio obtained from the experiment shall indicate the extent of uniform damage. However, there are two points of intersection, which can be resolved by solving Eq. (20a), for both the points and estimating the true extent of damage and its magnitude. The previous cases (e) and (f), which have given a ratio of 0.58 and 0.76 are solved and the damage extent is estimated as 30% and 20%, respectively.

9. Experimental program—axial rod

Towards experimental validation, two reinforced concrete beams are cast and tested. One has a uniform prismatic section and the other one has a constriction at the centre. These beams are tested in free–free longitudinal excitation mode. The beams had a depth of 150 mm, width of 150 mm and an overall length of 2500 mm. The damage was introduced as a reduction in width of beam to 100 mm for a length of 250 mm. The beams are nominally designed based on limit state theory. The cross section details of the beam are shown in Figs. 15(a) and (b).

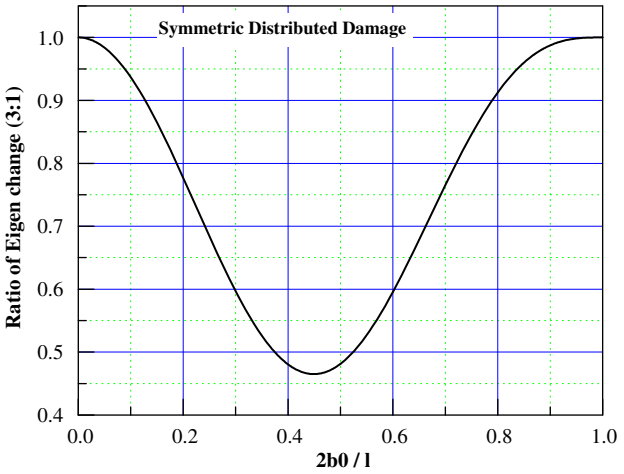

Fig. 14. Prediction of damage extent for a symmetrical distributed damage with Eigen_value-change_ratio between third and first modes.

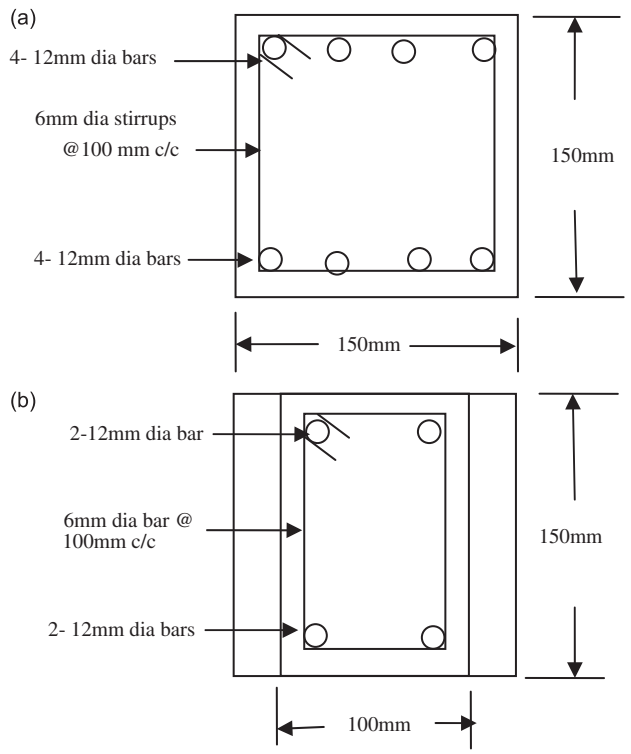

Fig 15. (a) Cross section of un-damaged portion of beam. (b) Cross section of damaged portion of beam.

9.1. Description of experimental set-up for axial rod

The beams are placed on two smooth G.I. pipes to get free–free condition in axial length direction. An acceleration pick up, a piezo-electric transducer is attached to one side of the beam to measure acceleration/velocity. An instrumented hammer with a steel tip and a piezo-electric force transducer is used to give the impact loading. The Oscilloscope records 2.5E+06 samples per sec and gives the output as plots of impact load and acceleration/velocity. The calibration values are

$$\text{Impact load}: \ 10\,\text{mV} = 1.0\,\text{N}$$

$$\text{Acceleration}: \ 10\,\text{mV} = 1\,\text{m/s}^2.$$

Impulsive load is applied in the axial direction using a hammer with different tips. Three tips used for the purpose are steel, plastic and rubber. The tips have tandem piezo-electric force transducer, which converts force into voltage and can be calibrated in force units. Fig. 16 shows the force inputs for the three tips and Table 1 give the variation in pulse widths for different hits.

9.2. Velocity of wave propagation

To find out the velocity of wave propagation, the pick up is placed on one side and load is applied at the other end of the un-damaged specimen. The difference in time between the hitting and the reaching of the wave at the other end is noted. Using known length of beam and the time taken by the wave to reach from one end of the beam to the other end, the velocity of wave propagation is found out. Fig. 17 shows the time delay between the trailing edge of force to the trailing edge of response. Wave velocity of axial wave propagation, worked out in this manner is found to be 3830 m/s.

9.3. Length of specimen—estimation

To find out the length of pile, load is applied at the same side where the pick up is placed (Un-damaged specimen). Time taken by the wave to come back after reflecting from the opposite end is noted. Using the velocity of wave propagation already deduced and using the time of travel by the wave through the beam the length of the beam is calculated. This works out to be 2420 mm.

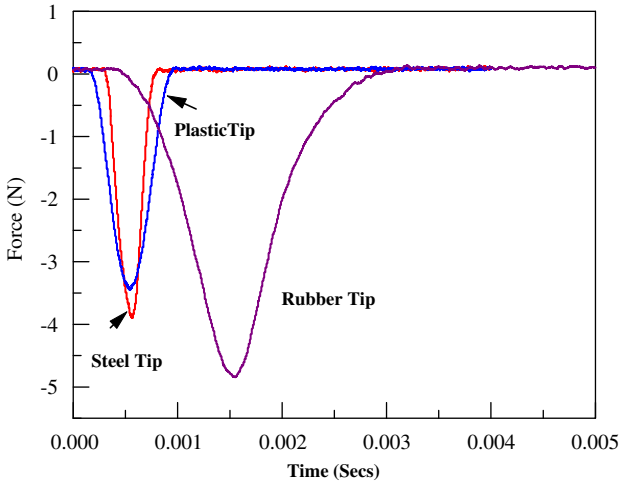

Fig. 16. Force profiles for different contact tips.

Table 1
Force pulse width for different tip materials.

Test trial no.	Pulse duration (μs)		
	Steel	Plastic	Rubber
1	466.50	740.30	2478.00
2	476.20	764.00	2449.00
3	462.80	738.50	2477.00
4	480.10	744.70	2501.00
5	480.30	748.70	2506.00

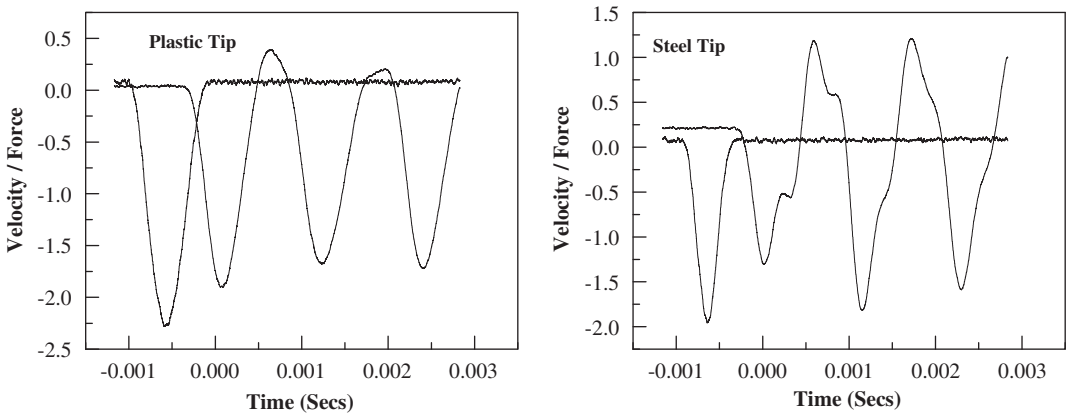

Fig. 17. Wave transit time delay between force and response situated at two ends.

9.4. *Response of test piece for different excitations*

Figs. 18–20 show the response of both the un-damaged and damaged specimens subjected to three kinds of half-sine loads due to contact of plastic, steel and rubber tips. Velocity time history is given as well as its frequency domain synthesis. The first observation is that the response is far different from the text-book type of response, with out pre-dominating wave propagation. The response is seemingly like a dynamic response and not of wave propagation response. Un-damaged beam exhibits a factor of 2.0 between the initial velocity response to the first reflected response (Fig. 18). The subsequent reflections diminish in amplitudes. Estimated damping is found to be 0.5–1%. Less damping is due to the free–free nature of beams and in actual foundation structures, larger damping can be expected.

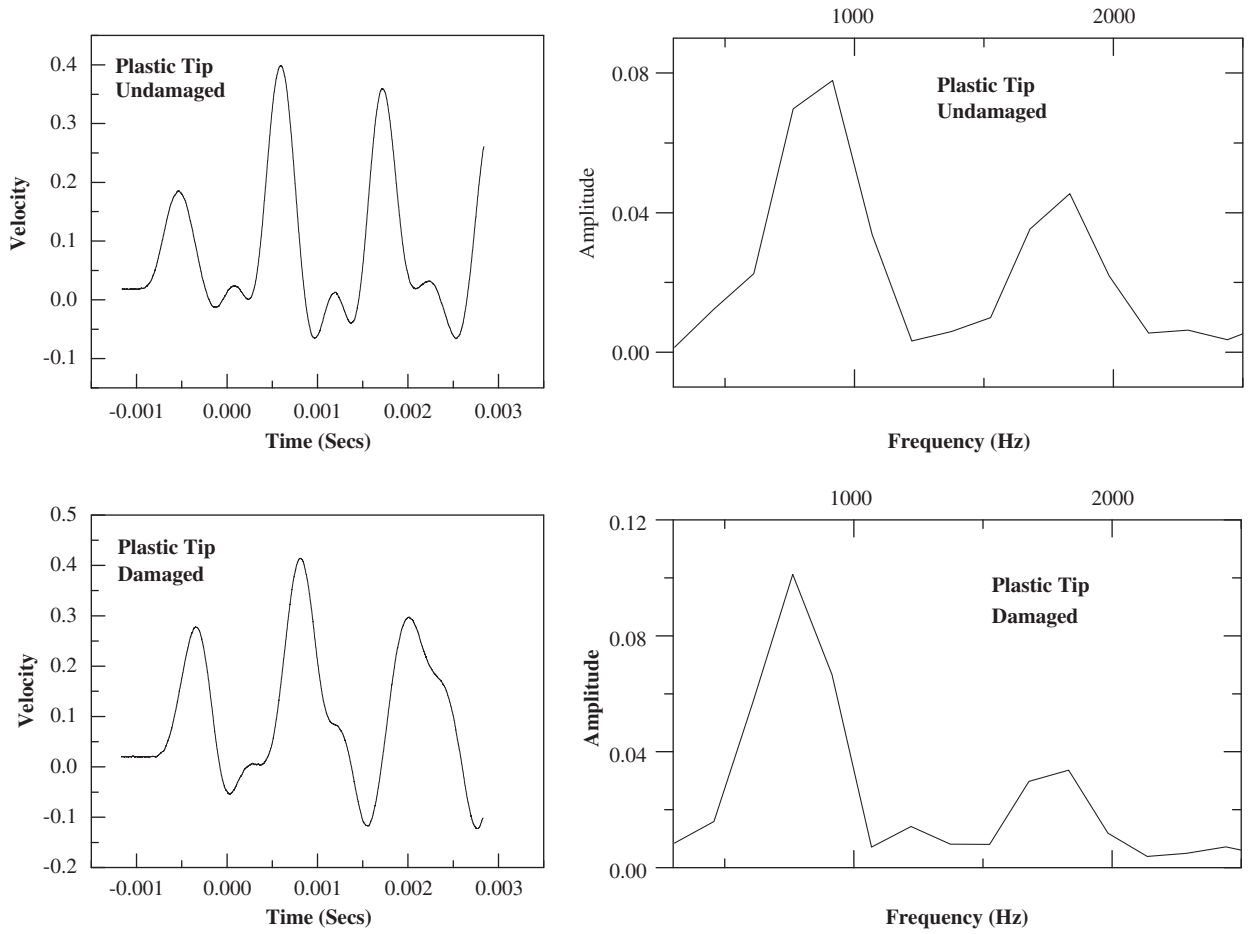

Fig. 18. Time history and FFT of velocity responses for un-damaged and damaged specimens—plastic tip.

Damaged beam exhibits a factor far less than 2.0 between the initial velocity response to the first reflected response and this may be due to the energy content in the initial response having been forked in two or more paths of reflections. (As the damping in the system is less. the energy is still preserved in the system to a large extent, for the first few cycles, but possibly available in other parts of the structure.) This may hold the clue of damage estimation from wave propagation, in a future work, and not merely depending on time history to follow the classical cases.

FFT response shows that rubber tip excites the fundamental mode only, plastic tip excites the first two modes and the steel tip excites the first three or four modes. This is understandable as more sharp the pulse width is, more of high frequency modes are excited. The frequencies excited by the impulsive force include 860, 1780, 2552 Hz for the un-damaged case and 761, 1733, 2408 and 3407 Hz, for the first three or more axial modes. The frequencies of a free–free rod are spaced at 1:2:3… and this is clearly seen. Strain energy density of the rod are more at centre for odd-numbered modes and less for even-numbered modes. Hence the Eigen value change is more for odd-numbered modes and less for even-numbered modes. Typical frequencies and mode shapes of free–free axial member is given as follows:

$$f_n = \frac{n}{2}\frac{V_p}{\ell} \quad \text{and} \quad \phi_n = \cos\frac{n\pi x}{l}$$

9.5. Analytical evaluation of damage for free–free axial rod used in the experiment

The damage simulated in the experiment using a free–free axial involves stiffness reduction as well as mass reduction. Damage is generally accompanied with loss of stiffness but the simultaneous loss of mass is rare and ‘necking’ in underground piles is the only example. Stiffness reduction causes a reduction in natural frequencies (or Eigen values), but the mass reduction causes an enhancement of natural frequencies. Hence both are compensating factors resulting in decreased sensitivity natural frequency to damage arising out of both mass and stiffness reduction. However towards getting an insight of the mechanics involved, the following expressions are derived and discussed.

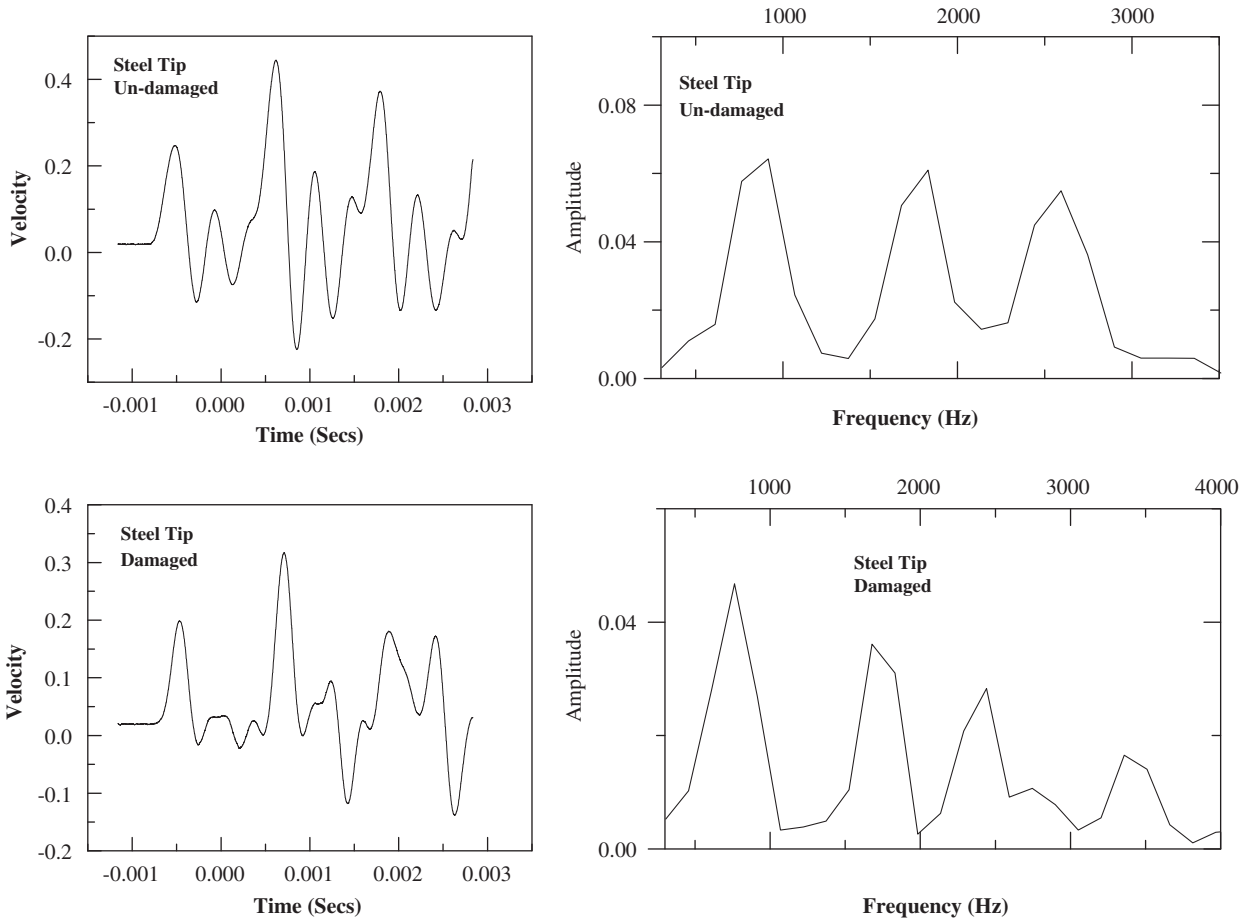

Fig. 19. Time history and FFT of velocity responses for un-damaged and damaged specimens—steel tip.

It is possible to derive the ratio of Eigen value change, in the '*n*-th' mode (factor-I) for a free–free axial rod due to stiffness loss alone quantified by reduction in the area of cross section:

$$\left[\frac{\Delta f_d^2}{f_{ud}^2}\right]_I = \beta\left[\frac{2b_0}{\ell} - \frac{1}{\pi\cdot n}\left\{\sin\frac{2\pi\cdot nb_0}{\ell}\cdot\cos\frac{2\pi\cdot n\ell_0}{\ell}\right\}\right] \tag{21a}$$

Similarly, the ratio of Eigen value change in the '*n*-th' mode (factor-II) due to mass reduction can be derived as follows:

$$\left[\frac{\Delta f_d^2}{f_{ud}^2}\right]_{II} = \beta\left[\frac{2b_0}{\ell} + \frac{1}{\pi\cdot n}\left\{\sin\frac{2\pi\cdot nb_0}{\ell}\cdot\cos\frac{2\pi\cdot n\ell_0}{\ell}\right\}\right] \tag{21b}$$

Combining both factors I and II, the effective Eigen value change can be written as

$$\left[\frac{\Delta f_d^2}{f_{ud}^2}\right]_{II} = -\beta\frac{2}{\pi\cdot n}\left\{\sin\frac{2\pi\cdot nb_0}{\ell}\cdot\cos\frac{2\pi\cdot n\ell_0}{\ell}\right\} \tag{21c}$$

It is seen from Eq. (21c), that the central damage accompanied with both mass and stiffness reduction in a free–free axial rod causes a decrease in natural frequencies for odd numbered modes (stiffness effect dominates) and increase in natural frequencies for even-numbered modes. However, if the extent of damage increases compared to the pseudo span length (distance between two successive nodes), this trend reverses.

Ratio of Eigen value changes between two modes can be derived as:

$$\frac{\left[\frac{\Delta f_d^2}{f_{ud}^2}\right]_n}{\left[\frac{\Delta f_d^2}{f_{ud}^2}\right]_m} = -\frac{m\cdot\left\{\sin\frac{2\pi\cdot nb_0}{\ell}\cdot\cos\frac{2\pi\cdot n\ell_0}{\ell}\right\}}{n\cdot\left\{\sin\frac{2\pi\cdot mb_0}{\ell}\cdot\cos\frac{2\pi\cdot m\ell_0}{\ell}\right\}} \tag{21d}$$

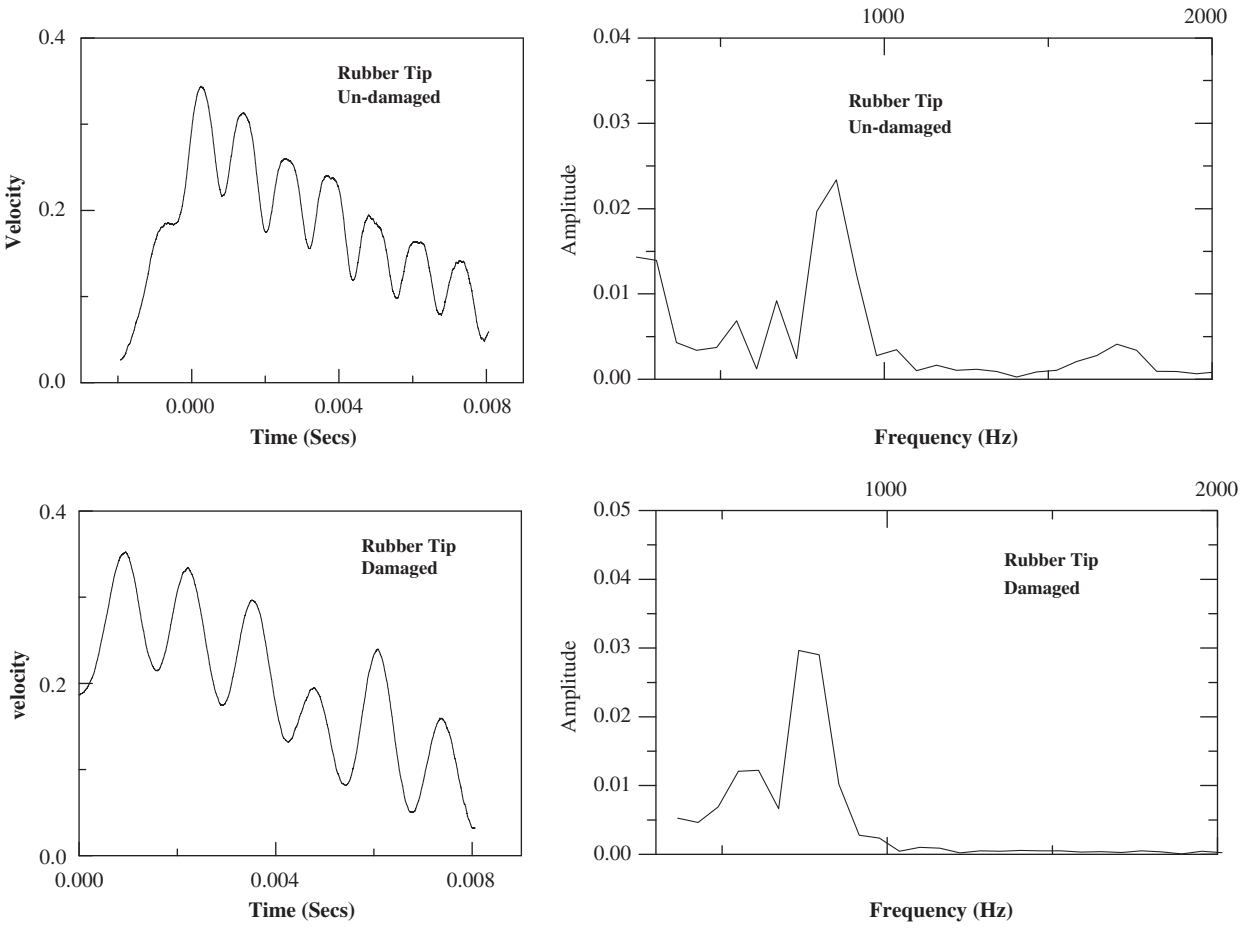

Fig. 20. Time history and FFT of velocity responses for un-damaged and damaged specimens—rubber tip.

If an a-priori information on the likelihood damage location is known as the centre of the member, then the information can be explicitly put in the equation and a simplified equation similar to Eq. (20) could be obtained:

$$\frac{\left[\dfrac{\Delta f_d^2}{f_{ud}^2}\right]_3}{\left[\dfrac{\Delta f_d^2}{f_{ud}^2}\right]_1} = -\frac{\left\{\sin\dfrac{6\pi\cdot b_0}{\ell}\right\}}{3\left\{\sin\dfrac{2\pi\cdot b_0}{\ell}\right\}} \tag{21e}$$

The equation is plotted in the form of a curve and shown in Fig. 21.

Further simplification of Eq. (21e) results in a straight forward equation for evaluation the extent of damage:

$$\frac{2b_0}{\ell} = \frac{1}{\pi}\sin^{-1}\left[\sqrt{0.75(1-\gamma)}\right]; \quad \gamma = \frac{\left[\dfrac{\Delta f_d^2}{f_{ud}^2}\right]_3}{\left[\dfrac{\Delta f_d^2}{f_{ud}^2}\right]_1} \tag{21f}$$

The first observation from the experimentally observed frequencies is that, there is a decrease for odd-numbered modes, but even modes do not show an increase but a marginal decrease. The reason is that, the stiffness reduction due to stress concentration and sharp corners, have rendered the effective area of the section lower than what is actually available. Hence the reduction of stiffness effects dominate rather than mass effect.

The position of damage is explicitly used in the analysis and the extent and the magnitude of damage are evaluated using Fig. 21. It is deduced that the damage magnitude at the central 21% length is 49% as against the actual area loss of 33%. It is re-iterated that the abrupt drop in axial area is actually equivalent to more loss of area, than what is simulated.

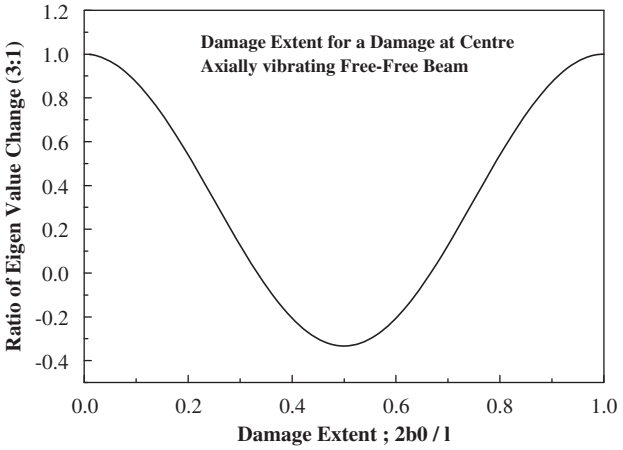

Fig. 21. Prediction of damage extent for a distributed damage at mid-length with Eigen_change_ratio between third and first modes—free–free beam.

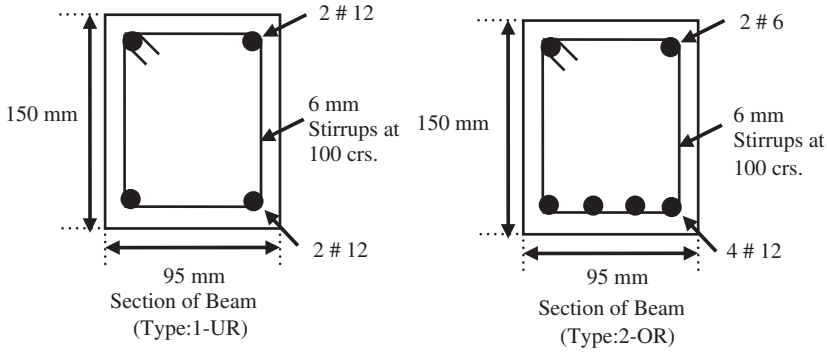

Fig. 22. Section details of RC beams tested.

10. Experimental program—flexural beam

With the necessary theoretical back-ground having been generated for a simply supported beam, the next logical step is the evaluation of the experimental performance of the damage detection algorithms. It is already seen that, Equal_Eigen_value-change contours lend themselves to a simple curve if a-priori information on the symmetrical damage is available.

Four reinforced concrete beams are tested in the laboratory with simply supported boundary conditions. These beams are divided into two sets, one pair for symmetrical loading, with a concentrated central load and the other pair for un-symmetrical loading with an off-centric loading. Hence the induced damages are either symmetric or un-symmetric. In each pair there are two beams, one with equal reinforcement at top and bottom (2#12), type-1, **UR**, and the other with more number of bottom bars (4#12) and two compression-side bars (2#6), type-2, **OR** to tie the reinforcement cage. The concrete is designed to be M25 (Characteristic Strength of 25 MPa) and the steels are of grade Fe-415 (Yield stress of 415 MPa). Fig. 22 shows the sections of the RC beam. The beams are subjected to various magnitudes of loads, starting from the virgin state to the theoretically calculated crack-initiation load, and two stages in-between the cracking and yielding stage, and a stage well beyond the yield stage (with constant load and large deflections). The applied load is measured with an in-built load cell of the Instron 50kN servo-hydraulic actuator and the central deflection is measured with a 0.01 mm precision Mitutoyo dial gauge. After each stage of loading, the beams are un-loaded and the natural frequencies and mode shapes are measured. The test arrangement consists of dynamic measurement, using a B&K-4370 accelerometer, B&K piezo-electric based force transducers, two B&K-2635 charge amplifiers for conditioning these signals and an AND dual channel FFT analyser for computing the frequency response function of the acceleration response with reference to the force input. Dynamic force is applied through a Philips 30N electro-dynamic spring-loaded shaker, which is energized by a power amplifier with sinusoidal signal from a signal generator. Measurements are made at 29 locations each separated by 100 mm, by the rowing accelerometer. Resonances are identified by the quadrature response of (Imaginary component) FRF at different points. Fig. 23 shows the typical cracked profile of the tested beams, under symmetrical and un-symmetrical load conditions.

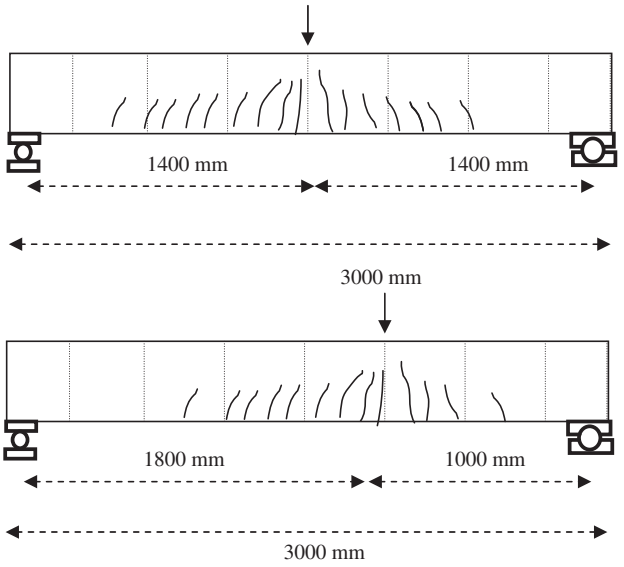

Fig. 23. Typical damage patterns in the symmetrically and un-symmetrically damaged beams.

Table 2
Variation of natural frequencies for symmetrically damaged beams.

Flexural mode	Beam—type-1 (UR) (Frequencies—Hz)					Beam—type-2 (OR) (Frequencies—Hz)				
	Virgin state	DS1	DS2	DS3	DS4	Virgin state	DS1	DS2	DS3	DS4
Applied load (kN)	0	2.4	7.0	14.0	14.0[a]	0	2.4	7.0	14.0	26.0[a]
1	30.00	29.125	27.575	26.325	19.33	29.50	28.38	26.83	26.13	19.83
2	108.75	108.25	106.25	99.625	79.50	107.00	106.23	103.15	102.50	90.75
3	270.00	264.00	256.75	251.95	193.85	270.00	263.0	255.40	250.56	215.63
4	422.50	417.38	404.325	389.25	332.53	425.00	417.63	403.50	399.30	345.45

Note: DS indicates damage states after application of loads.
[a] Load remains same but displacement is a larger value.

Table 3
Variation of natural frequencies for un-symmetrically damaged beams.

Flexural mode	Beam—type-1 (UR) (Frequencies—Hz)					Beam—type-2 (OR) (Frequencies—Hz)		
	Virgin state	DS1	DS2	DS3	DS4	Virgin state	DS1	DS2
Applied load (kN)	0	2.4	7.0	12.4	12.4[a]	0	7.0	26
1	30.00	29.75	28.25	28.15	24.50	30.00	29.40	25.98
2	108.50	107.75	103.27	100.00	90.00	107.00	105.40	93.85
3	270.00	269.88	258.88	256.00	229.60	269.00	268.5	239.88
4	428.00	424.00	408.00	400.83	359.30	425.00	417.13	376.30

Note: DS indicates damage states after application of loads.
[a] Load remains same but displacement is a larger value.

10.1. Discussion on experimental results of flexural beam

Table 2 gives the de-generation of the condition of the RC beams from an initial un-cracked state to various damage states, subjected to progressively increasing central concentrated loads, with reduction in flexural natural frequency as the indicator of damage. The state of damage is symmetric for both the sets of beams. The beam-type-2 (OR) by virtue of its larger reinforcement ratio has higher load capacity as evinced by its ultimate load capacity (26 kN). Various flexural modes are identified by the mode shapes, which are also measured from the imaginary part of FRF, which however is not discussed here. The first observation is that, applied load alone cannot be a good indicator of damage. DS3 and DS4 states, for beam-type-1 show such a big difference in frequencies for same load but for different irrecoverable energy levels.

Hence the damage state as indicated by the drop in frequencies is more related with the energy lost from the system rather than the load applied. Table 3 gives the condition of the un-symmetrically damaged beams of both types under varying damage states.

For symmetrically damaged beams with a centrally located contiguous damage, the method of Equal_Eigen value_change contours is initially applied and the position of the damage is found to be at the mid-position or very

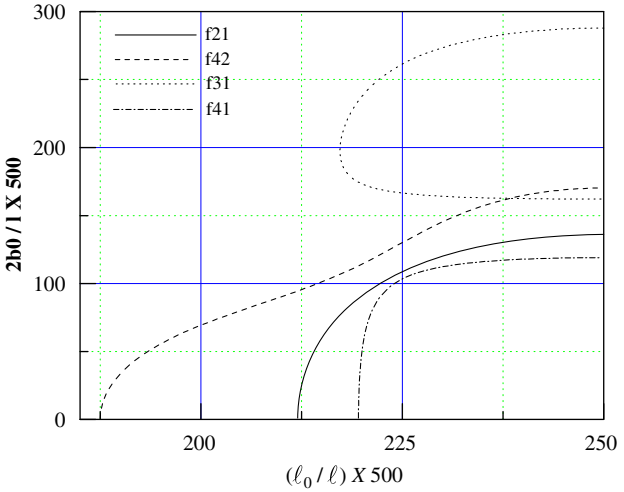

Fig. 24. Typical Iso_Eigen-Change contours for the experimental beam (Type-1, UR, DS-1).

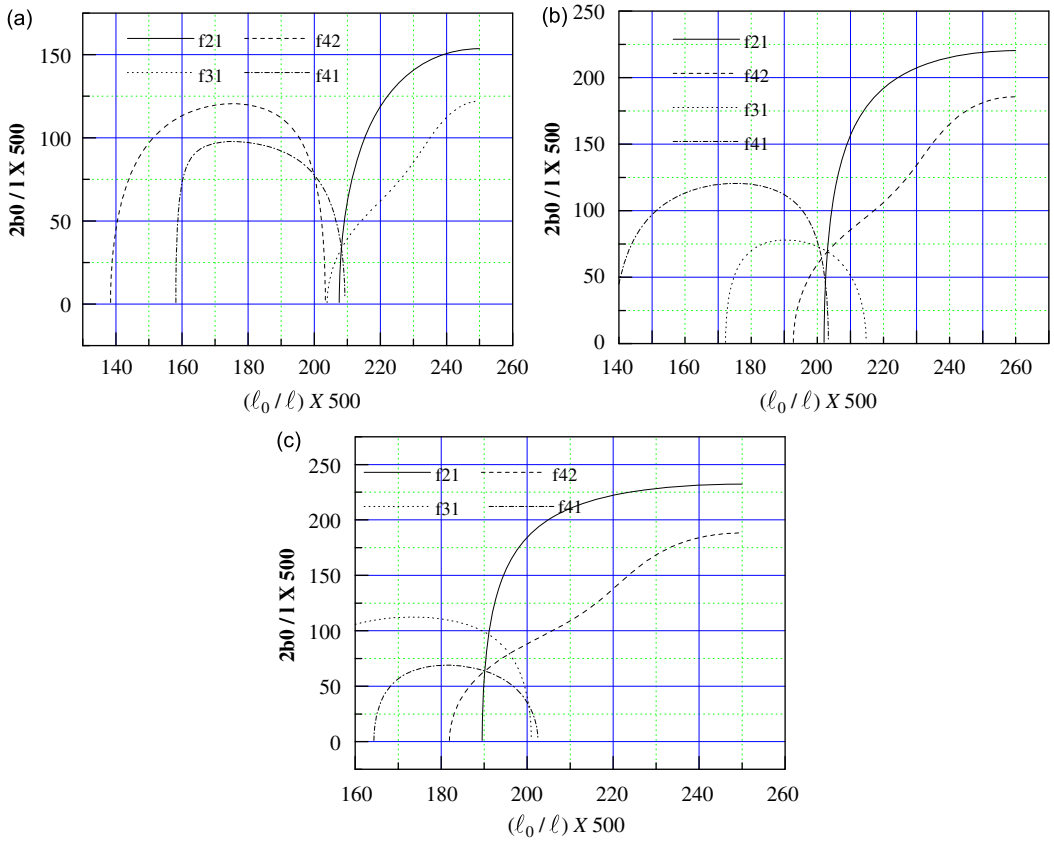

Fig. 25. Experimental damage identification using Iso_Eigen change contours for un-symmetrically damaged beams: (a), (b) Type-1 (UR), DS1 and DS2, (c) Type-2 (OR), DS1.

close to the centre. Fig. 24 shows the identification of symmetrical damage location from Iso-Eigen_value_change contour. However larger scatter is seen in the curve for the extent of damage.

Fig. 25 shows the identification of typical un-symmetrical damage location from Equal_Eigen-change contours. Though the actual damage location is 0.36ℓ, from one end of the beam, the results of the contour plot show variation ranging from 0.36–0.42 times ℓ. As in the symmetrical case, a scatter is seen in the extent of damage also.

11. Conclusions

The method of damage identification from Equal_Eigen-value-change contours gives good results in locating the position of a damaged zone, irrespective of the initial assumption, that the damage should be constant in the affected segment. The cancellation of the damage magnitude in deriving the relevant expressions, indicates that it shall be in-variant with reference to β (magnitude of damage) for a large extent of β. An elegant simple equation is brought out as a result of further simplification on a centrally located, symmetric, contiguous damage for a flexural, simply supported beam. The third and first mode information is sufficient to get the information on damage extent and magnitude.

Once the location of damage is identified, further experiments using local damage detection parameters like strain and curvature can be employed in an elaborate experimental program. Also, repair methodologies can be planned. The experiment conducted on an axial response of a beam and simply supported reinforced concrete beam have given encouraging results and further work is in progress in this direction for other structural elements.

Acknowledgement

The paper is published with the approval of Director, SERC. Also, the comments and encouragement of the peer reviewers for this paper and the connected previous papers have helped in re-shaping the direction of thinking of authors. The third author acknowledges the tacit guidance of Guru Ramana and the Maha Periyava of Kanchi.

References

[1] P. Cawley, R.D. Adams, The location of defects in structures from measurements of natural frequencies, *Journal of Strain Analysis* 14 (1979) 49–57.
[2] A. Morassi, Identification of a crack in a rod based on changes in a pair of natural frequencies, *Journal of Sound and Vibration* 242 (2001) 577–596.
[3] M. Palacz, M. Krawczuk, Analysis of longitudinal wave propagation in a cracked rod by the spectral element method, *Computers and Structures* 80 (2002) 1809–1816.
[4] M. Palacz, M. Krawczuk, Vibration parameters for damage detection in structures, *Journal of Sound and Vibration* 249 (2002) 999–1010.
[5] M. Krawczuk, J. Grabowska, M. Palacz, Longitudinal wave propagation—Part-II, Analysis of crack influence, *Journal of Sound and Vibration* 295 (2006) 479–490.
[6] M. Krawczuk, M. Palacz, W. Ostachowicz, The dynamic analysis of a cracked Timoshenko beam by the spectral element method, *Journal of Sound and Vibration* 264 (2003) 1139–1153.
[7] M. Krawczuk, Application of spectral beam finite element with a crack and iterative search technique for damage detection, *Finite Elements in Analysis and Design* 38 (2002) 537–548.
[8] G.M.L. Gladwell, *Inverse Problems in Vibration*, second ed., Kluwer Academic Publishers, Dordrecht, 2004.
[9] S.W. Doebling, C.R. Farrar, M.B. Prime, P.W. Shevitz, *Damage Identification. Health Monitoring of Structural and Mechanical Systems from Changes in their Vibration Characteristics—A Literature Review*, Los Alamos National Laboratory, Los Alamos, New Mexico, 1996.
[10] G.M. Owolabi, A.S.J. Swamidas, R. Seshadri, Crack detection in beams using changes in frequencies and amplitudes of frequency response functions, *Journal of Sound and Vibration* 265 (2003) 1–22.
[11] X.F. Yang, A.S.J. Swamidas, R. Seshadri, Crack identification in vibrating beams using the energy-based method, *Journal of Sound and Vibration* 244 (2) (2001) 339–357.
[12] J.M.M. Silva, A.J.M.A. Gomes, Experimental dynamic analysis of cracked free–free beams, *Journal of Experimental Mechanics* 30 (1) (1994) 20–25.
[13] F. Ju, M. Mimovich, Modal frequency method in diagnosis of fracture damage in structures, *Proceeding of the Fourth International Modal Analysis Conference*, Los Angeles, CA, 1986, pp. 1423–1429.
[14] M.R. Choudhury, M. Ramirez, A comparison of the modal responses for a defective versus non-defective concrete test beams, *Proceedings of the 10th International Modal Analysis Conference*, San Diego, CA, 1992, pp. 508–515.
[15] M.B. Prime, D.W. Shevitz, Linear and non-linear methods for detecting cracks in beams, *Proceeding of 14th International Modal Analysis Conference*, Honolulu, 1996, pp. 1437–1443.
[16] N. Lakshmanan, P. Srinivasulu, V.S. Parameswaran, Post cracking stiffness and damping in reinforced concrete beam elements, *Journal of Structural Engineering, India* 17 (4) (1991) 1405–1411.
[17] N. Rajagopalan, N. Lakshmanan, C.A. Jeyasehar, Damage assessment in reinforced concrete beams using natural frequencies, *Journal of Structural Engineering, India* 26 (3) (1999) 165–172.
[18] S. Hassiotis, G.D. Jeong, Assessment of structural damage from natural frequency measurements, *Computers and Structures* 49 (4) (1993) 679–691.
[19] S. Hassiotis, Identification of damage using natural frequencies and Markov parameters, *Computers and Structures* 74 (2000) 365–373.
[20] N. Lakshmanan, B.K. Raghuprasad, K. Muthumani, N. Gopalakrishnan, D. Basu, Wavelet analysis and enhanced damage indicators, *Smart Structures and System—An International Journal* 3 (2007) 23–49.
[21] N. Lakshmanan, B.K. Raghuprasad, K. Muthumani, N. Gopalakrishnan, R. Sreekala, Seismic damage estimation through measurable dynamic characteristics, *Computers and Concrete—An International Journal* 4 (2007) 167–186.
[22] N. Lakshmanan, B.K. Raghuprasad, K. Muthumani, N. Gopalakrishnan, D. Basu, Damage evaluation through radial basis function network (RBFN) based artificial neural network scheme, *Smart Structures and System—An International Journal* 4 (2008) 23–49.
[23] N. Lakshmanan, B.K. Raghuprasad, K. Muthumani, N. Gopalakrishnan, D. Basu, Identification of reinforced concrete beam-like structures subjected to distribute damage from experimental static measurements, *Computers and Concrete—An International Journal* 5 (2008) 70–90.
[24] L. Yu, L. Cheng, L.H. Yam, Y.J. Yan, Application of Eigen value perturbation theory for detecting small structural damage using dynamic responses, *Composite Structures* 78 (2007) 402–409.
[25] P.L. Gatti, V. Ferrari, *Applied Structural and Mechanical Vibrations, Theory, Methods and Measuring Instrumentations*, E&F.N Spon, London, 1999.